Modulation of the selectivity of CO2 to CO electroreduction in palladium rich Palladium-Indium nanoparticles

Supporting Information

Modulation of the selectivity of CO_2 to CO electroreduction in Palladium rich Palladium-Indium nanoparticles

Davide Pavesi,[a,b] Federico Dattila,[c] Rim C. J. Van de Poll,[d] Dimitra Anastasiadou,[d] Rodrigo García-Muelas,[c] Marta Figueiredo,[d] Gert-Jan M. Gruter,[a,e] Núria López,[c*] Marc T. M. Koper,[b] Klaas Jan P. Schouten[a,*, ∩]

[a]*Avantium Chemicals BV, Zekeringstraat 29 1014 BV Amsterdam, The Netherlands*

[b]*Leiden Institute of Chemistry, Leiden University, PO Box 9502, 2300 RA, Leiden, The Netherlands*

[c]*Institute of Chemical Research of Catalonia (ICIQ), The Barcelona Institute of Science and Technology (BIST), Av. Països Catalans 16. 43007 Tarragona, Spain.*

[d]*Inorganic Materials and Catalysis, Eindhoven University of Technology, P.O. Box 513, 5600 MB Eindhoven, The Netherlands*

[e]*Van 't Hoff Institute for Molecular Sciences, University of Amsterdam, PO Box 94157, 1090 GD Amsterdam, The Netherlands*

[∩]*Current address: Teijin Aramid BV, Tivolilaan 50, 6824 BW Arnhem, The Netherlands*

[*]E-mail: nlopez@iciq.es; KlaasJan.Schouten@teijinaramid.com

Computational Details

Stability of the Pd_xIn_y systems. Initially, we performed structural optimization of Pd, In, the intermetallics PdIn, Pd_2In, Pd_3In, and solid solutions of In in Pd of approximate composition $Pd_{98}In_2$ and $Pd_{90}In_{10}$ (at.%). The crystal structures for the intermetallic compounds were retrieved from literature.[1,2,3,4] Models from solid Pd-In solutions were generated taking as base the Pd fcc conventional cell. The $Pd_{98}In_2$ composition was modelled from the 2×2×3 expansions of bulk Pd, containing 48 atoms, and replacing one of them by In. The $Pd_{90}In_{10}$ composition was modeled from the 2×2×2 expansion, containing 32 atoms, and replacing three non-adjacent Pd atoms by In. This allowed to find the correct lattice parameter and calculate the enthalpy of formation (ΔH_f) of the intermetallic compounds and solid solutions according to Equation S1. E_{Pd+In} is the energy calculated for the Pd_xIn_y bulk cell *via* density functional theory (DFT), N_{Pd+In} is the total number of atoms in the cell, N_{In} and N_{Pd} are, respectively, the number of In and Pd atoms in the cell, E_{In} and E_{Pd} are, respectively, the DFT energies of an In or Pd atom in their bulk structures.

$$\Delta \boldsymbol{H_f} = \frac{\boldsymbol{E_{Pd+In}}}{\boldsymbol{N_{Pd+In}}} - \frac{\boldsymbol{N_{In}}}{\boldsymbol{N_{Pd+In}}} * \boldsymbol{E_{In}} - \frac{\boldsymbol{N_{Pd}}}{\boldsymbol{N_{Pd+In}}} * \boldsymbol{E_{Pd}} \quad \textbf{(S1)}$$

The values obtained are summarized in Table S3 and compared to experimental values of solid solutions of similar compositions and intermetallic compounds.[1] Overall, DFT calculated formation energies are comparable with experimental enthalpies, even though they present a systematic offset of about 20%. The formation of Pd-In solid solutions and intermetallic compounds is thermodynamically favorable and the compounds are stable.

Given the very different surface energies of In and Pd (0.29 J m^{-2} for In(001) vs. 1.37 J m^{-2} for Pd(111), lowest energy termination for these metals) and the much larger thermodynamic drive for In to be oxidized, upon air exposure In could possibly migrate to the nanoparticles surface and segregate. However, our experimental results suggest otherwise. The XRD of $Pd_{98}In_2$/C and $Pd_{90}In_{10}$/C (Fig. 3) suggests that In is still incorporated in the Pd lattice, at least partially and the XPS analysis confirms that indium is in its metallic state in these two catalysts (Fig. S5). Moreover, the separation and surface segregation of In, at least in the more In-rich $Pd_{50}In_{50}$/C, could result in a relatively thick In surface layer which should be detectable in the cyclic voltammetry. On the contrary, the cyclic voltammogram of $Pd_{50}In_{50}$/C (Fig. 2) presents a distinct shape, not traceable to either Pd or In, suggesting that intermetallic compounds with a different structure, stoichiometry, and electronic properties are stable on the surface. The exothermicity of the Pd-In bonds seems to be enough to stabilize the structures against segregation. Besides, whatever the behavior of the bimetallic systems may be upon air exposure, the reducing conditions imposed during electrolysis could change the situation drastically, as the potentials investigated in this study are well below the redox potentials of In and Pd.

To check whether solid solutions of In in Pd would be stable against a competing ordered intermetallic phase we calculated enthalpies for the demixing of the solid solutions (s.s.) into pure Pd + Pd-In intermetallics (Fig. S7). Demixing enthalpies were calculated according to the stoichiometry of the following reactions, Equations S2-S7:

$$\mathbf{Pd_{29}In_3(s.s.) \rightarrow Pd_{26} + 3PdIn} \quad \textbf{(S2)}$$

$$\mathbf{Pd_{29}In_3(s.s.) \rightarrow Pd_{23} + 3Pd_2In} \quad \textbf{(S3)}$$

$$\mathbf{Pd_{29}In_3(s.s.) \rightarrow Pd_{20} + 3Pd_3In} \quad \textbf{(S4)}$$

$$\mathbf{Pd_{47}In_1(s.s.) \rightarrow Pd_{46} + PdIn} \quad \textbf{(S5)}$$

$$\mathbf{Pd_{47}In_1(s.s.) \rightarrow Pd_{45} + Pd_2In} \quad \textbf{(S6)}$$

$$\mathbf{Pd_{47}In_1(s.s.) \rightarrow Pd_{44} + Pd_3In} \quad \textbf{(S7)}$$

The only thermodynamically favorable process is the demixing of In-Pd solid solution into pure Pd and ordered Pd_3In. For $Pd_{47}In$ this reaction is only slightly exothermic (–0.08 eV $atom^{-1}$), whilst for increased indium content, $Pd_{29}In_3$, there is a significant thermodynamic drive for the decomposition of the solid solution (–0.24 eV $atom^{-1}$). This is in line with the Pd-In phase diagram. The formation of solid solutions or intermetallic compounds are competing processes and the formation of intermetallic compounds becomes dominant beyond a certain In concentration.

The stability of the Pd-In solid solutions against segregation and islanding of In atoms was investigated according to a systematic approach previously applied.[5] We modelled 4-layers, 64 atoms Pd(111) slabs with the topmost two layers allowed to relax, with 1 or more In substituents in different arrangements. This allowed to estimate the tendency of In to segregate on the surface and to form islands as opposed to being isolated and surrounded by Pd atoms. The results are reported in Fig. S8 and suggest that In atoms in the Pd matrix

have a slight tendency to be on the surface (even before accounting for the larger oxygen affinity of In), rather than being in the bulk or forming near surface alloys (NSA). Also, In prefers being surrounded by Pd atoms, rather than forming islands.

Adsorption of relevant intermediates. For the investigation of the catalytic properties of the synthesized nanoparticles, we initially determined the most stable surfaces of Pd, In and the intermetallic compounds by optimizing different surface terminations. The values of the surface energy for the investigated surfaces are reported in Table S5. Then, we assessed intermediates adsorption on the most stable surfaces, expected to be the most abundant facets on nanoparticles according to Wulff theorem.[6,7] For the Pd-In solid solution we used a Pd(111) slab with one In atom on the surface.

Attenuated Total Reflectance (ATR) Spectroscopy

Methodology. Fig. 4 in the main text shows the ATR spectra of the five catalysts in a gaseous atmosphere of CO (on the left) and after purging with Ar (right) to allow desorption of weakly adsorbed CO. Before adsorbing CO, the catalysts were pre-reduced in a pure H_2 atmosphere for 45 minutes. This reduction procedure is enough to reduce Pd oxide, since it can be reduced by hydrogen below room temperature even in dilute hydrogen streams,[8] but not to reduce oxidized In, which remains in its oxide form even under high temperature and hydrogen pressures.[9,10] Our XPS analysis of the In 3d orbitals (Fig. S5) shows that while pure In nanoparticles are fully oxidized, the In in $Pd_{98}In_2$/C and $Pd_{90}In_{10}$/C is fully metallic, indicating that incorporation in the Pd lattice can protect In atoms from oxidation. Thus, the reduction treatment should be effective also for these catalysts. The situation is more complicated for $Pd_{50}In_{50}$/C because the In peak in this catalyst roughly coincides with the one of In^{3+}. This could mean that the In in the particles is fully oxidized, but also that the interaction with Pd is dramatically altering its electronic structure. In any case, since during bulk electrolysis the $Pd_{50}In_{50}$/C does not behave like any of the parent metals, we conclude that even if In is fully oxidized before the reaction, it would alloy with Pd during reduction (or else, if a thick In shell would have remained during electrochemical reaction, the catalyst behavior should be similar to pure In both in CVs and electrolysis).

Band assignment. For palladium, infrared bands in the range of 2060-2100 cm^{-1} are normally assigned to linear-bound *CO, while bands in the range between 1750-2000 cm^{-1} are assigned to bridged and multi-bonded *CO.[11] The bands in the spectra in Fig. 4 are a convolution of hollow and bridge sites (more intense band) and top sites (less intense band) on the different adsorption sites present on the nanoparticles, such as terraces, steps, corners, and defects. The slightly different adsorption energies on similar sites (for example a bridge bonded *CO on a terrace or an edge), cause the broadening of the peaks.

Pd/C, $Pd_{98}In_2$/C and $Pd_{90}In_{10}$/C show very similar spectra. Specifically, Pd/C and $Pd_{98}In_2$/C behave very similarly both in CO atmosphere and after Ar stripping. There does not seem to be a significant peak shift, meaning that the average CO adsorption energy is constant. In addition to this, the bands look qualitatively the same, indicating that the binding mode is also analogous. Since the peaks here represent a convolution of several similar adsorption modes, it is difficult to highlight small alterations in the adsorption geometry. In order to identify possible differences, we integrated the “hollow + bridge” band and the “top” band

and plotted the ratio “top”/”hollow+bridge” (Fig. S6). From this analysis we find that Pd/C and $Pd_{98}In_2$/C show the same ratios in both CO and Ar. $Pd_{90}In_{10}$/C instead has a significantly higher ratio of top sites in CO atmosphere. After stripping with Ar the spectrum becomes similar to the other two Pd-rich catalysts, indicating that $Pd_{90}In_{10}$ may possess some additional CO adsorption sites which bind the molecule more weakly and could be separate from the strong binding sites which cause surface poisoning. These strongly adsorbing sites could instead be analogous to the ones on the other two catalysts, suggesting that this material may be composed of patches of Pd-In solid solution (similar reactivity as $Pd_{98}In_2$/C and Pd/C) and intermetallic compounds with a different adsorption behavior. This would be in agreement with the Pd-In phase diagram, since the composition is beyond the solubility limit of In in Pd, thus enabling the formation of intermetallic compounds.

The CO adsorption behavior in the gas phase of $Pd_{50}In_{50}$/C is comparable with previously reported catalysts with similar composition. The formation of the intermetallic compound PdIn with a CsCl structure and fully isolated Pd atoms leads to exclusive adsorption of CO on top of the isolated Pd atoms.[12] In our case only a weak CO vibration is detected, which could be either a red-shifted on-top or a blue shifted bridge adsorption site. This suggests that intermetallic compounds presenting different surface reactivity may be formed, at least after the reducing treatment. In does not show any CO adsorption, as expected since In catalyst should be present as In oxide, and this element does not adsorb CO even in the metallic state.

Supplementary Tables

Table S1. Atomic % composition of the catalysts from SEM-EDX and XPS. Estimated metal loading on the electrodes used in the study.

Catalyst	Composition / at.%				Electrode metal loading / mg cm^{-2}
	SEM-EDX		XPS		
	In	Pd	In	Pd	
In/C	100	0	100	0	0.16
$Pd_{50}In_{50}$/C	53.1 ± 4.9	46.9 ± 4.0	45.59	54.41	0.11
$Pd_{90}In_{10}$/C	10.5 ± 1.4	89.5 ± 1.4	10.01	89.99	0.14
$Pd_{98}In_{2}$/C	n.d.	100	2.97	97.03	0.13
Pd/C	0	100	0	100	0.12

Table S2. Average particle size from TEM pictures.

Catalyst	Particle size from TEM / nm
In/C	3.6 ± 0.9
$Pd_{50}In_{50}$/C	3.7 ± 0.4
$Pd_{90}In_{10}$/C	3.8 ± 1.0
$Pd_{98}In_{2}$/C	4.1 ± 1.0
Pd/C	4.4 ± 1.2

Table S3. Formation enthalpy (ΔH_f) of Pd-In solid solutions and intermetallic compounds. $Pd_{47}In$ and $Pd_{29}In_3$ are models of solid solutions (s.s.), while the remaining models are of Pd-In intermetallic phases (IMC). Beyond a certain In concentration, the systems show a tendency to form intermetallic compounds rather than solid solutions, as expected from the Pd-In phase diagram.

	ΔH_f / eV atom^{-1}	
	This study	**Experimental**[13]
$Pd_{47}In$ (s.s.)	–0.04	–0.05
$Pd_{29}In_3$ (s.s.)	–0.17	–0.21
Pd_3In (IMC)	–0.47	–0.55
Pd_2In (IMC)	–0.52	–0.63
PdIn (IMC)	–0.51	–0.63

Table S4. Crystal structures and lattice parameters of the model crystals resulting from DFT calculations.

Crystal structure	**Lattice parameters**
In: tetragonal	a = 3.25 Å; c = 4.94 Å
Pd: fcc	a = 3.94 Å
PdIn: cubic	a = 3.31 Å
Pd_2In: orthorhombic	a = 4.24 Å; b = 5.72 Å; c = 8.39 Å
Pd_3In: tetragonal	a = 4.11 Å; c = 7.74 Å
Pd-In solid solution	$d_{Pd\text{-}In}$ = 3.97 Å

Table S5. DFT-calculated surface energies for different facets of pure In and Pd and intermetallic compounds. The In-t and Pd-t denominations stand for a surface terminated with either In only or Pd only. The most stable surfaces are highlighted in bold.

Surface	γ / J m^{-2}
In (001)	**0.28**
In (010)	0.36
In (100)	0.36
In (110)	0.39
In (111)	0.44
PdIn (100)	1.27
PdIn (110)	**0.72**
PdIn (111)-In-t	1.05
PdIn (111)	0.80
Pd_2In (010)	**1.17**
Pd_2In (110)	1.20
Pd_2In (111)	1.27
Pd_3In (100)	**1.31**
Pd_3In (110)	1.41
Pd_3In (110)-Pd-t	1.37
Pd (100)	1.55
Pd (110)	1.63
Pd (111)	**1.37**

Table S6. Binding energies for different adsorption configurations on the investigated intermetallic compounds, In and Pd. Specific adsorption sites are reported within brackets, whilst ss subscript stands for subsurface atom.

Surface	Adsorbate	ΔE_{DFT} / eV Sites		
		Top	Bridge	Hollow
Pd(111)	**H**			–0.69
	CO			–1.54
	COOH	–0.36		
Pd_3In(100)	**H**		+0.35 (Pd-Pd)	–0.66 (4Pd Pd_{ss}) –0.27 (4Pd In_{ss})
	CO	–0.77(Pd)	–1.10 (Pd-Pd)	–1.44 (4Pd Pd_{ss}) –0.98 (4Pd In_{ss})
	COOH	+0.52(In) –0.12(Pd)		
Pd_2In(010)	**H**			–0.48 (3Pd In_{ss})
	CO	–0.67(Pd)	–0.95 (Pd-Pd)	–0.96 (3Pd Pd_{ss}) –1.02 (3Pd In_{ss})
	COOH	+0.38 (In) –0.24 (Pd)		
PdIn(110)	**H**	+0.75 (In) +0.21(Pd)		+0.82(2In 2Pd Pd_{ss}) +0.08(2In 2Pd In_{ss})
	CO	+0.59 (In) +0.00 (Pd)		+0.63(2In 2Pd Pd_{ss}) +0.68(2In 2Pd In_{ss})
	COOH	+0.56 (In) +0.07(Pd)		
In(001)	**H**			+0.76
	CO		+0.52	
	COOH	+0.31		

Supplementary Figures

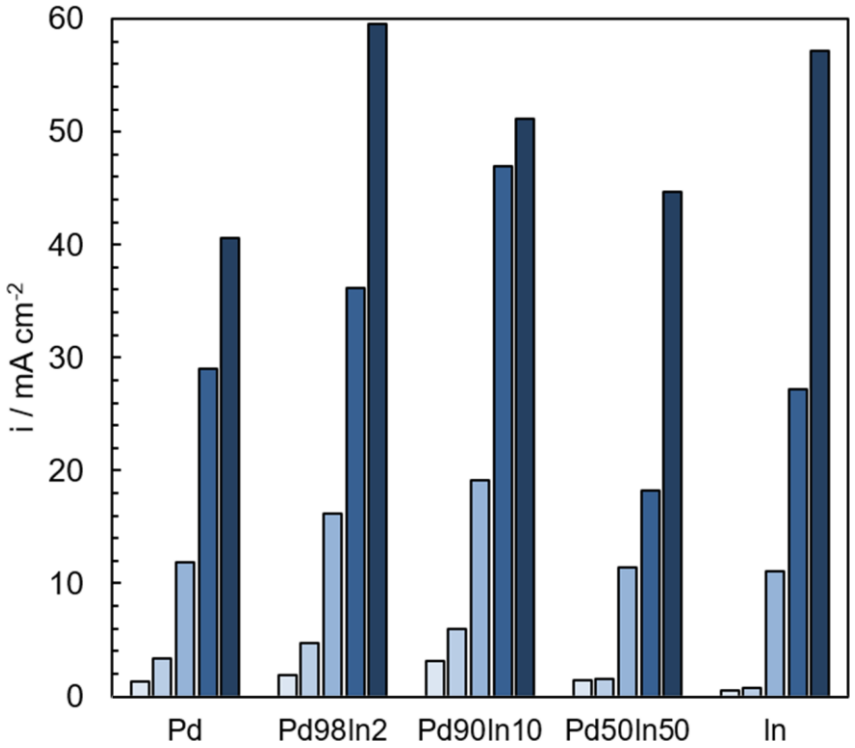

Figure S1. Average geometrical current densities recorded during bulk electrolysis. Progressively darker blue indicates progressively more negative applied potential.

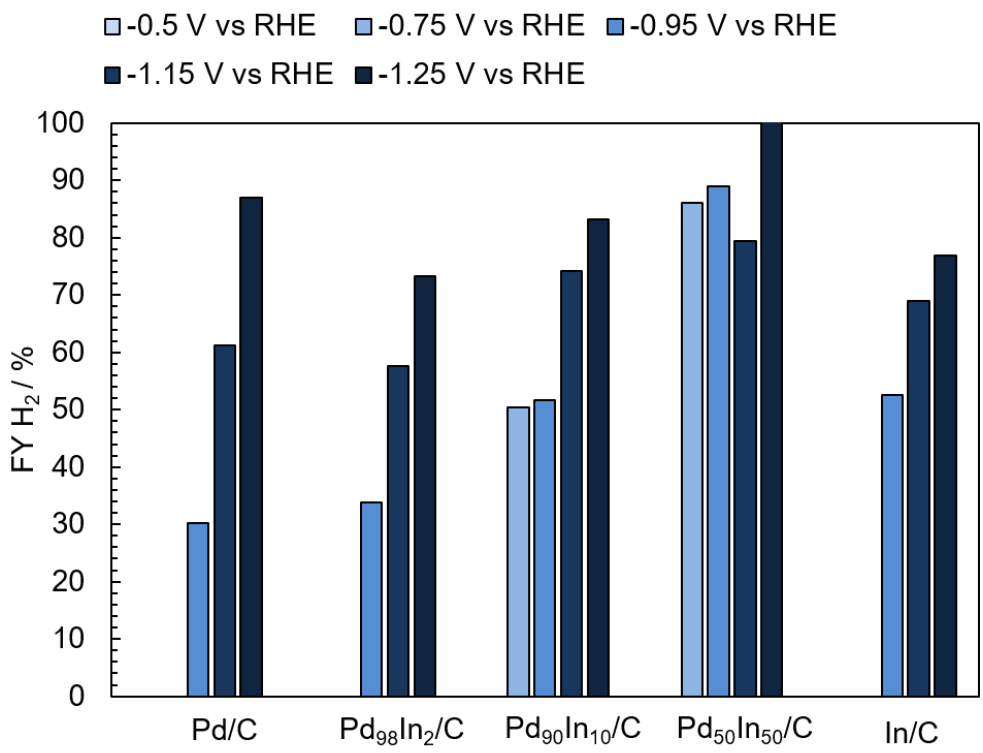

Figure S2. Faradaic yields towards hydrogen of the 5 catalysts. The value at –0.5 V and in some cases at –0.75 V could not be calculated due to small quantities of the gas being evolved, below the detection limit of the instrument. Due to possible interference of the He carrier gas in the H_2 peak, these values may be less accurate than the Faradaic yields toward CO.

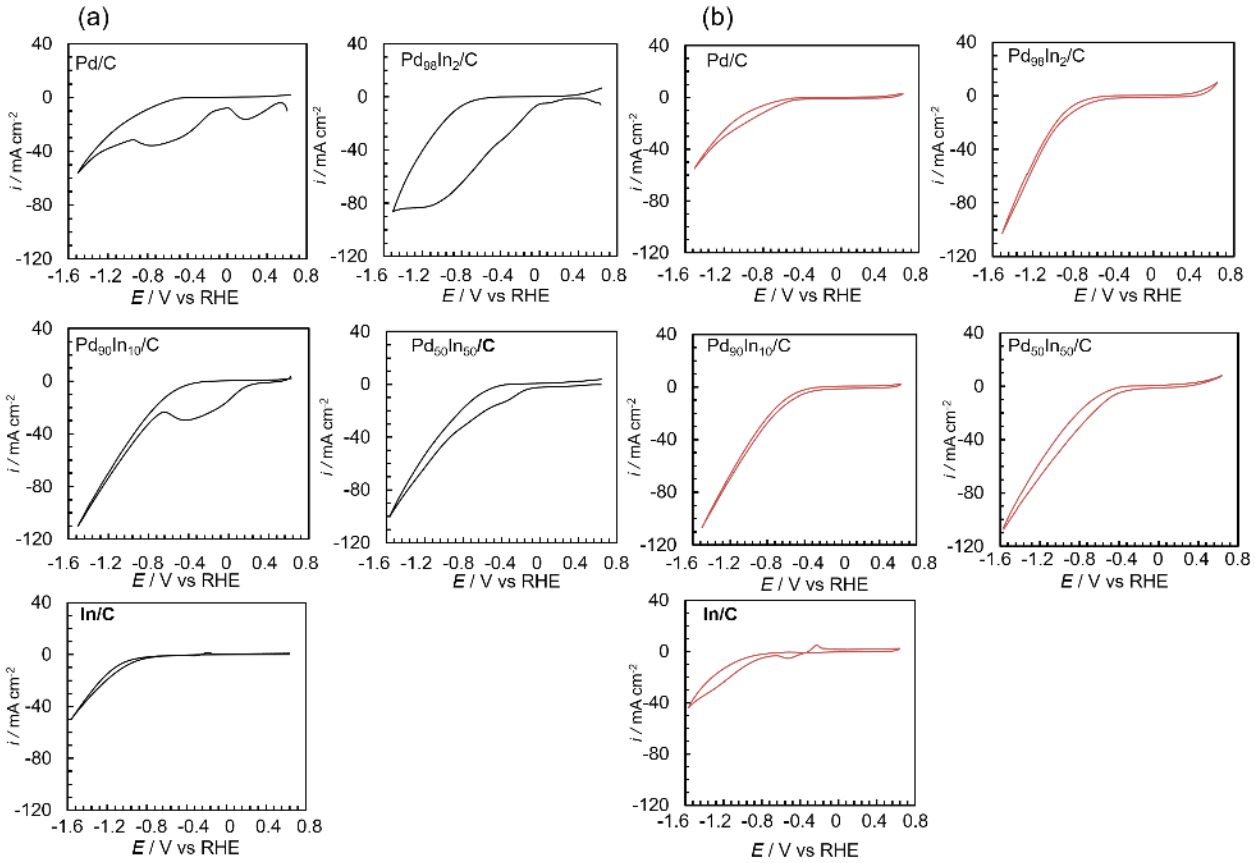

Figure S3. Voltammetric responses in 0.5 M $KHCO_3$, CO_2 saturated between –1.5 V and +0.6 V to avoid CO re-oxidation: (a) first cycle, CO adsorption is visible; (b) from the second cycle the CVs do not show CO adsorption peaks, confirming the presence of surface sites susceptible to CO poisoning for Pd/C, $Pd_{98}In_2$/C and $Pd_{90}In_{10}$/C.

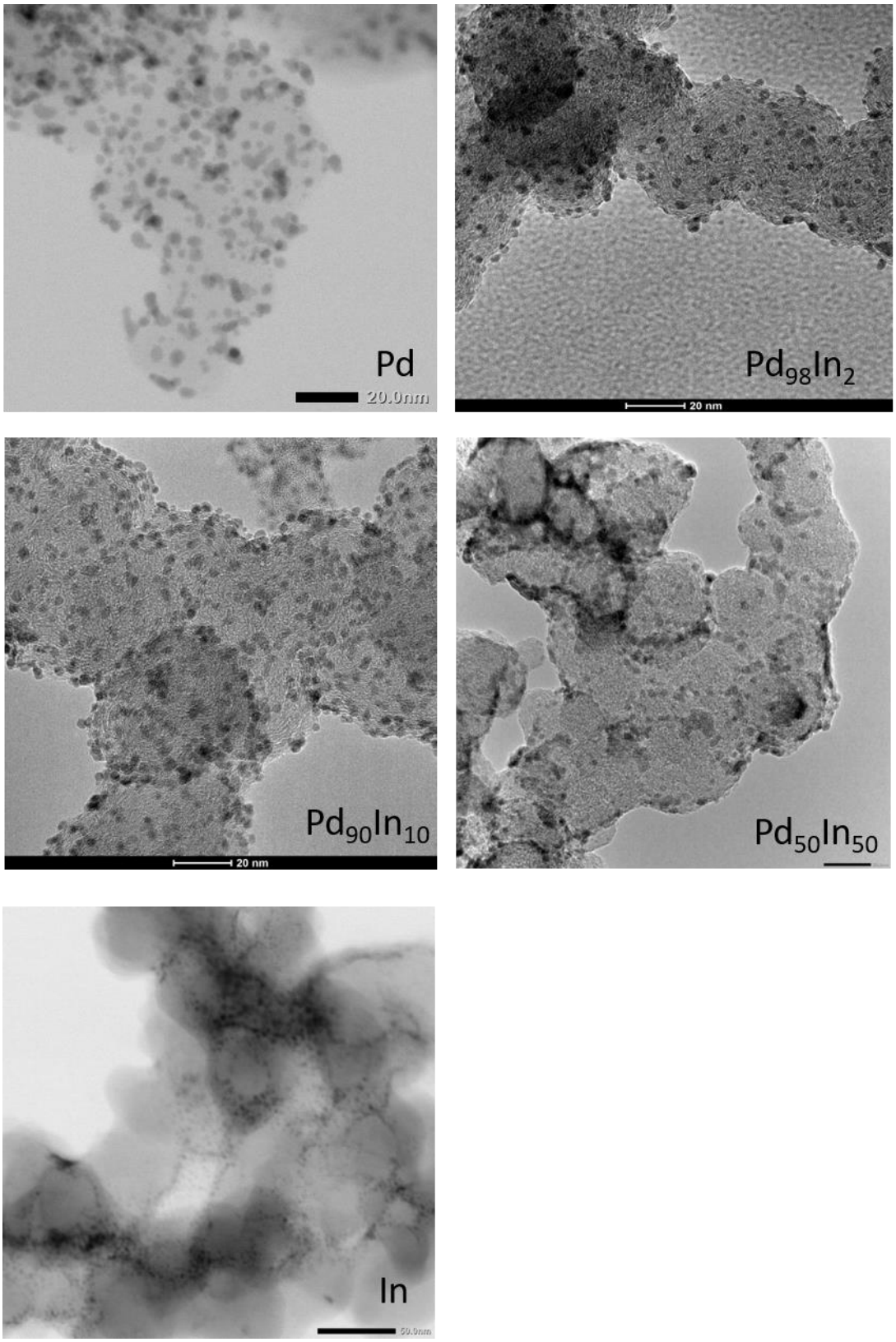

Figure S4. Representative TEM pictures of the investigated nanoparticles.

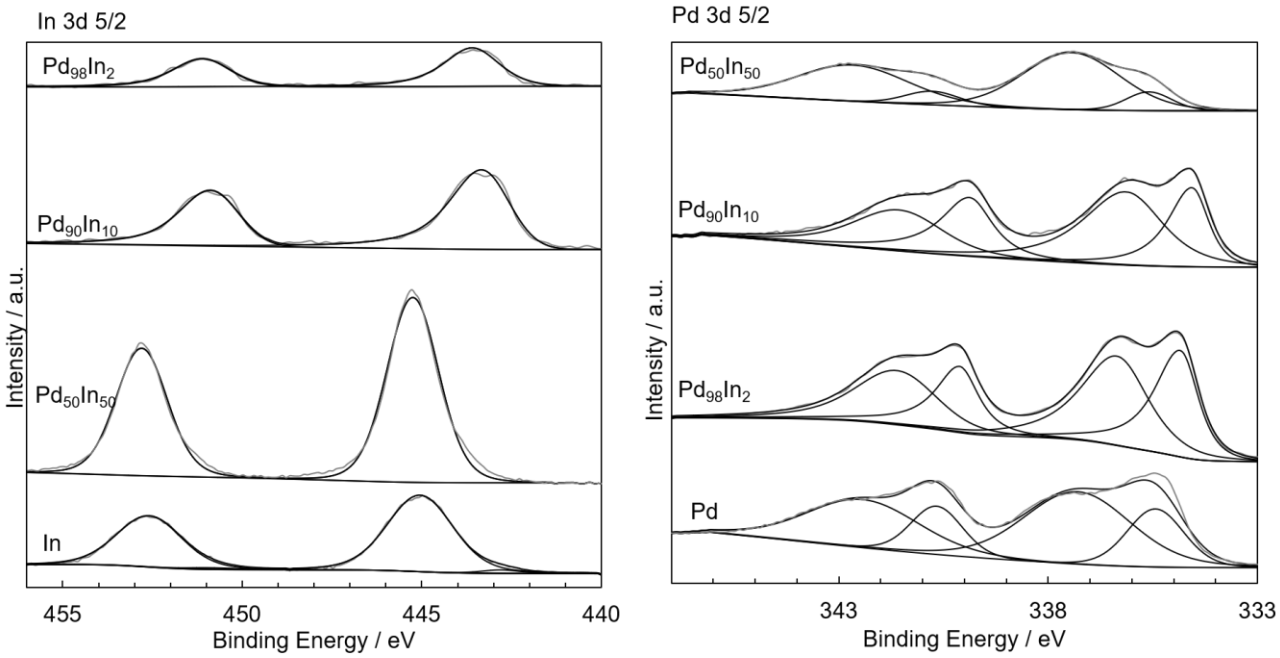

	In 3d 5/2	Pd^0 3d 5/2	Pd^{2+} 3d 5/2
In	445.33	–	–
$Pd_{50}In_{50}$	445.25	335.59	337.44
$Pd_{90}In_{10}$	443.34	334.57	336.13
$Pd_{98}In_2$	443.6	334.84	336.34
Pd	–	335.44	337.3

Figure S5. XPS spectra of the investigated catalysts. In 3d (left) and Pd 3d (right). Peak positions (maxima in eV) are summarized in the table.

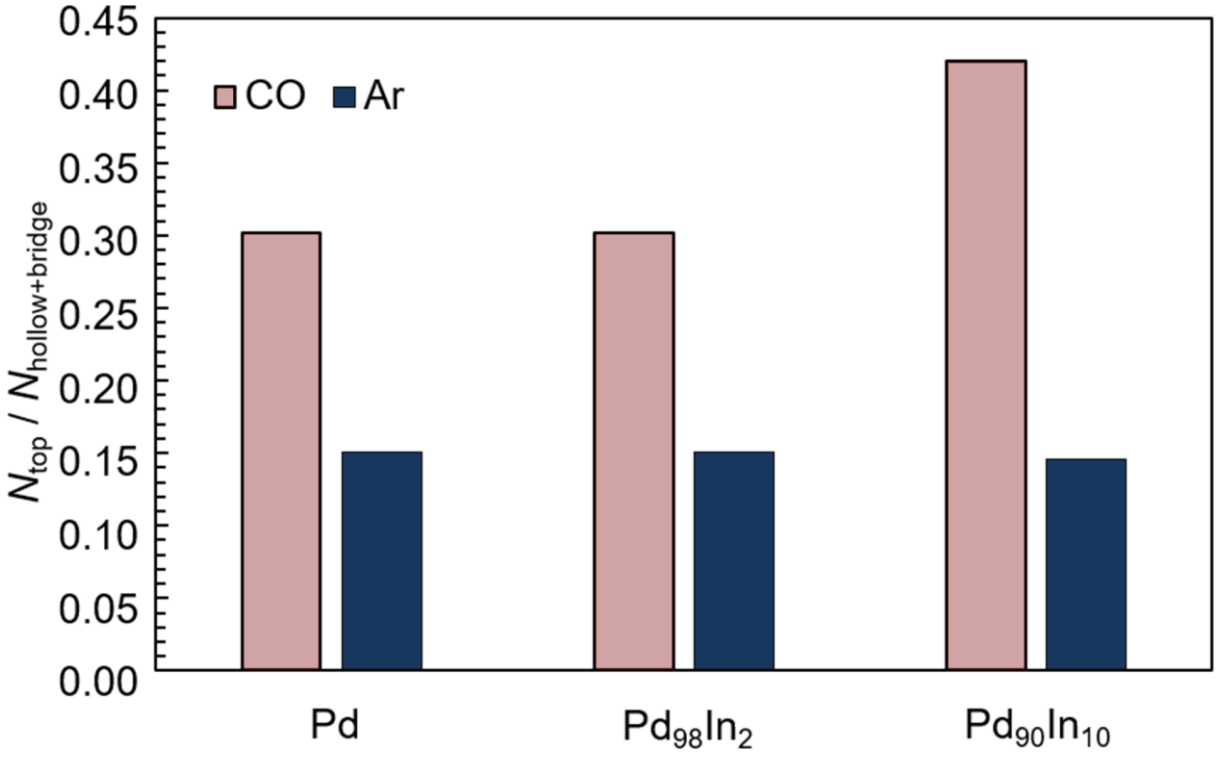

Figure S6. Ratio of the area of top sites divided by the area of hollow + bridge sites on the the Pd-rich catalysts in CO atmosphere (light red bars, related to reversibly + irreversibly adsorbed *CO) and after Ar stripping (blue bars, only irreversibly adsorbed *CO), calculated from Fig. S3.

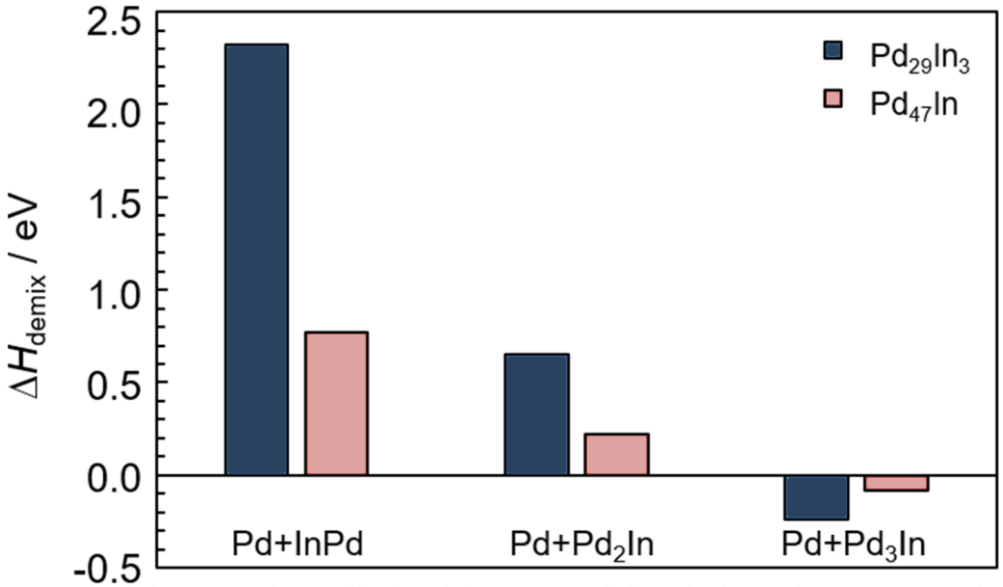

Figure S7. Enthalpies for the full demixing of solid solutions into pure Pd + ordered intermetallic phases.

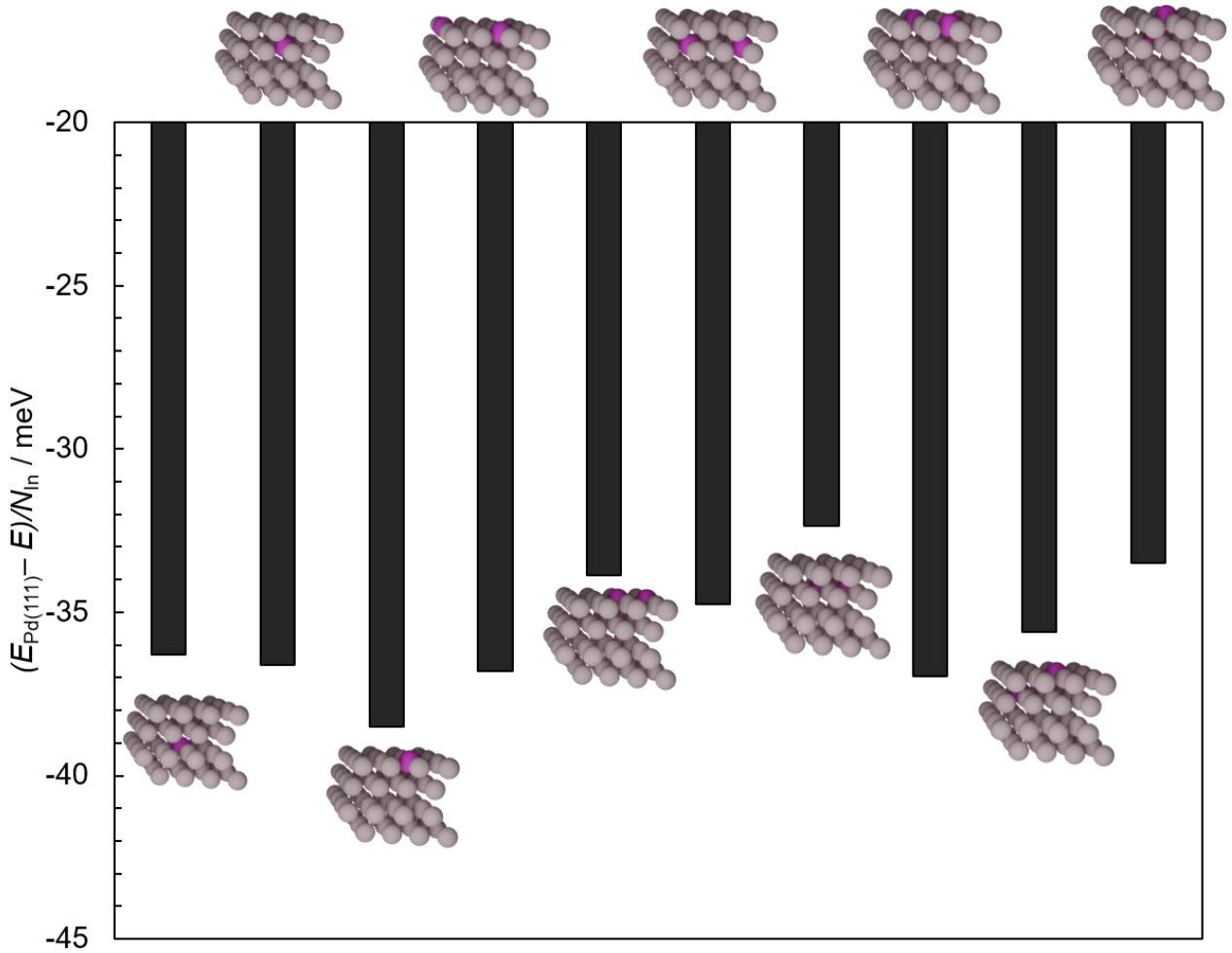

Figure S8. Formation energy for different In substitution configurations in (4×4) Pd(111) vs energy of an analogous (4×4) Pd(111) slab normalized by the number of substitutions, N_{In}. Overall, In-Pd solid solutions present lower formation energies than pure Pd and In has a slight tendency to be isolated on the surface. Pd atoms are shown in gray, In atoms in purple. From left to right we have the following models: bulk In atom, In as near-surface-alloy (NSA), surface In atom, 2 surface In atoms separated by 2 Pd atoms, 2 adjacent surface In atoms, 2 NSA In atoms separated by 1 Pd atom, 2 adjacent NSA In atoms, 2 surface In atoms separated by 1 Pd atom, 1 surface In atom and 1 NSA In atom (non-adjacent), 1 surface In atom and 1 NSA In atom.

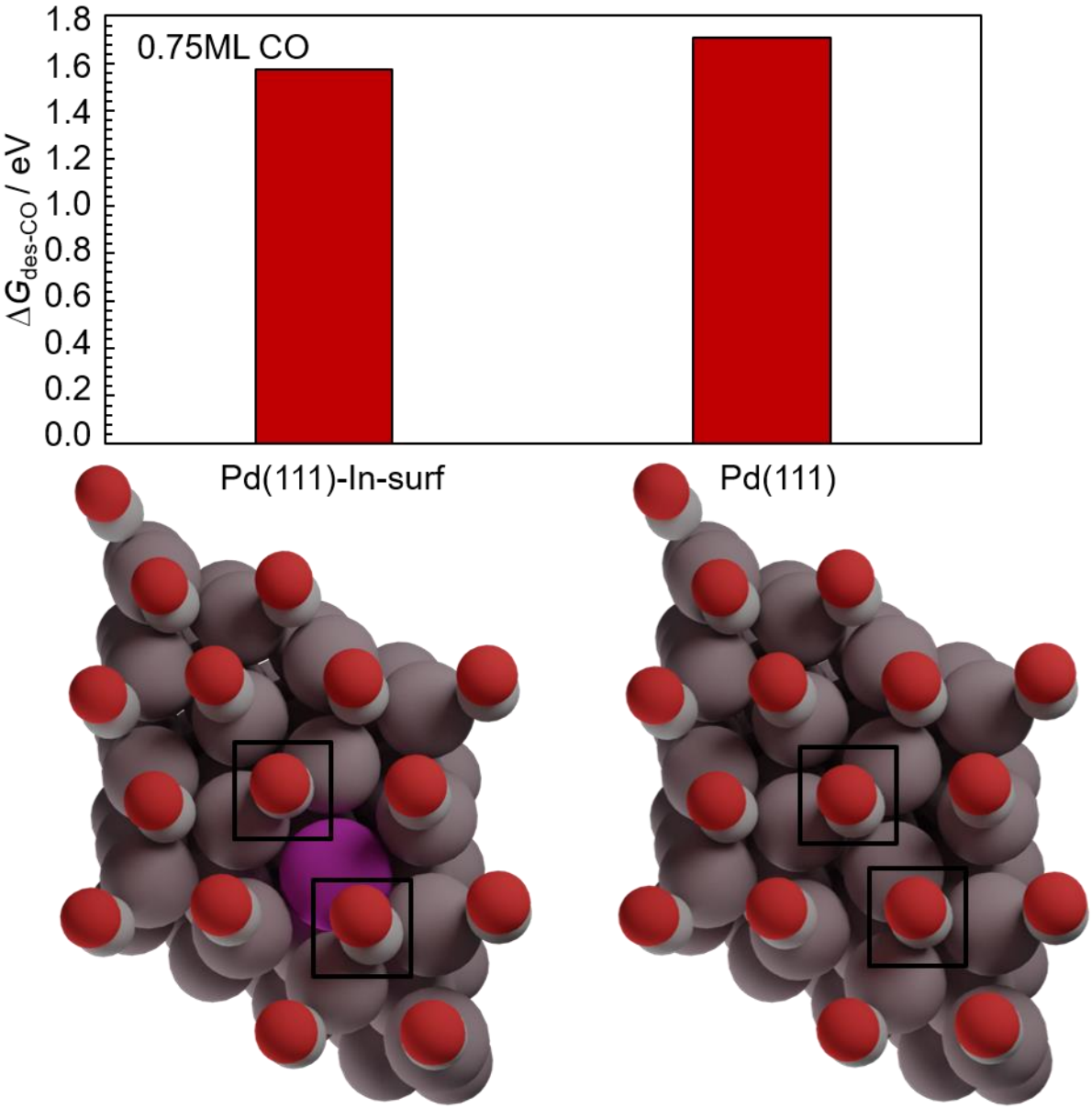

Figure S9. Average CO desorption energies at high CO coverage (0.75 ML) on Pd(111) and a Pd-In solid solution surface. Average binding energy and the binding mode does not change significantly between the systems. The two CO molecules close to the positively charged In substituent are repelled and pushed from a hollow to a bridge site on the Pd-In surface (see black squared insets). The differential desorption energy for the CO molecules in the frame is: +1.49 eV for the pure Pd system, +0.18 eV for the Pd-In system for a CO molecule on a 2Pd1In hollow site, and +1.14 eV for a *CO molecule adsorbed on a bridge site. The last adsorption configuration is the lowest in energy since it minimizes the electrostatic repulsion on the Pd-In surface.

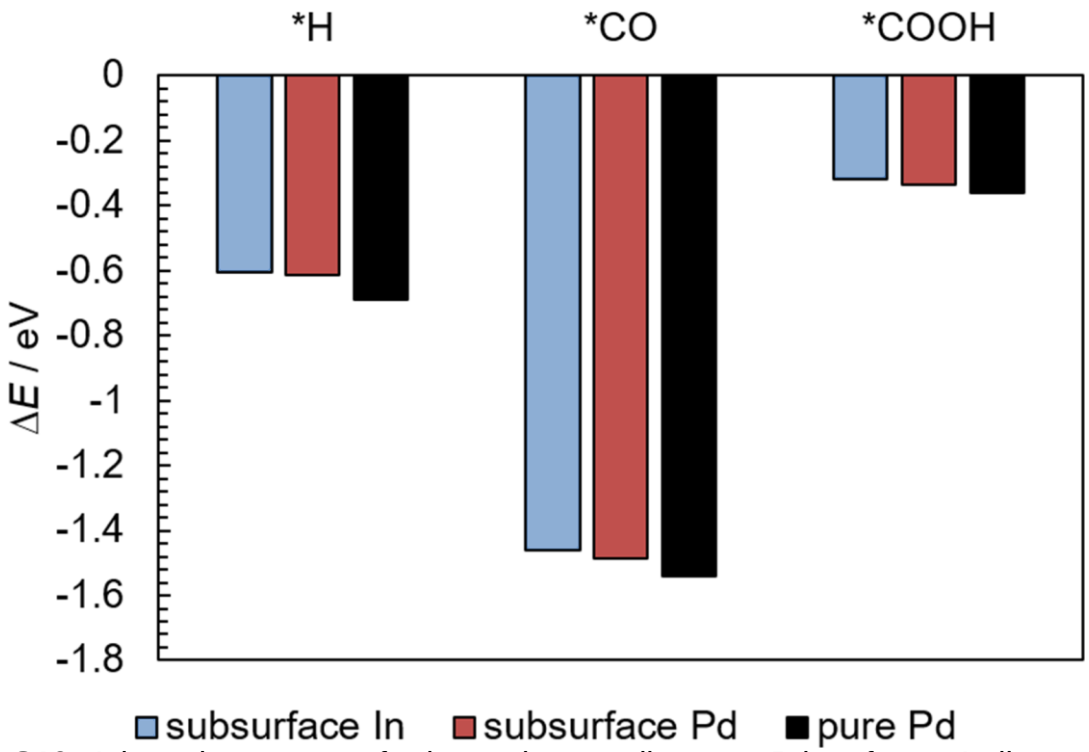

Figure S10. Adsorption energy of relevant intermediates on Pd surfaces. Indium atoms, if present, are in the subsurface. In light blue, binding energies when the adsorbate is placed in proximity of a subsurface In. In red, binding energies when the adsorbate is placed far away from the subsurface In. In black, binding energies on a pure Pd slab. The adsorption properties of systems with subsurface In atoms do not change significantly compared to pure Pd, since the Pd matrix screens electronic effects due to In. In affects surface reactivity only if present at the surface.

References

(1) Okamoto, H. In-Pd (Indium-Palladium). *J. Phase Equilibria*, 2003, 24, 481.

(2) Kohlmann, H. & Ritter, C. Reaction Pathways in the Formation of Intermetallic $InPd_3$ Polymorphs. *Zeitschrift für Anorg. und Allg. Chemie*, 2009, 635, 1573–1579.

(3) Kohlmann, H. & Ritter, C. Refinement of the crystal structures of palladium-rich in-Pd compounds by X-ray and neutron powder diffraction. *Zeitschrift fur Naturforsch. - Sect. B J. Chem. Sci.*, 2007, 62, 929–934.

(4) Harris, I. R., Norman, M. & Bryant, A. W. A study of some palladium-indium, platinum-indium and platinum-tin alloys. *J. Less-Common Met.*, 1968, 16, 427–440.

(5) López, N. & Vargas-Fuentes, C. Promoters in the Hydrogenation of Alkynes in Mixtures: Insights from Density Functional Theory. *Chem. Commun.*, 2012, 48, 1379–1391.

(6) Wulff, G. XXV. Zur Frage der Geschwindigkeit des Wachsthums und der Auflösung der Krystallflächen. *Zeitschrift für Krist. - Cryst. Mater.*, 1901, 34, 449–530.

(7) Carchini, G., Almora-Barrios, N., Revilla-López, G., Bellarosa, L., García-Muelas, R., García-Melchor, M., Pogodin, S., Błoński, P. & López, N. How theoretical simulations can address the structure and activity of nanoparticles. *Top. Catal.*, 2013, 56, 1262–1272.

(8) Chou, C. W., Chu, S. J., Chiang, H. J., Huang, C. Y., Lee, C. J., Sheen, S. R., Perng, T. P. & Yeh, C. T. Temperature-programmed reduction study on calcination of nano-palladium. *J. Phys. Chem. B*, 2001, 105, 9113–9117.

(9) Frei, M. S., Capdevila-Cortada, M., García-Muelas, R., Mondelli, C., López, N., Stewart, J. A., Curulla Ferré, D. & Pérez-Ramírez, J. Mechanism and microkinetics of methanol synthesis via CO_2 hydrogenation on indium oxide. *J. Catal.*, 2018, 361, 313–321.

(10) Martin, O., Martín, A. J., Mondelli, C., Mitchell, S., Segawa, T. F., Hauert, R., Drouilly, C., Curulla-Ferré, D. & Pérez-Ramírez, J. Indium oxide as a superior catalyst for methanol synthesis by CO_2 hydrogenation. *Angew. Chemie - Int. Ed.*, 2016, 55, 6261–6265.

(11) Ebbesen, S. D., Mojet, B. L. & Lefferts, L. The influence of water and pH on adsorption and oxidation of CO on Pd/Al_2O_3-an investigation by attenuated total reflection infrared spectroscopy. *Phys. Chem. Chem. Phys.*, 2009, 11, 641–649.

(12) Wu, Z., Wegener, E. C., Tseng, H. T., Gallagher, J. R., Harris, J. W., Diaz, R. E., Ren, Y., Ribeiro, F. H. & Miller, J. T. Pd-In intermetallic alloy nanoparticles: Highly selective ethane dehydrogenation catalysts. *Catal. Sci. Technol.*, 2016, 6, 6965–6976.

(13) Amore, S., Delsante, S., Parodi, N. & Borzone, G. Thermochemistry of Pd–In, Pd–Sn and Pd–Zn alloy systems. *Thermochim. Acta*, 2009, 481, 1–6.